New Journal of Physics
The open-access journal for physics

Structural characterization of porous solids by simultaneously monitoring the low-temperature phase equilibria and diffusion of intrapore fluids using nuclear magnetic resonance

Daria Kondrashova, Muslim Dvoyashkin and Rustem Valiullin[1]
Institute of Experimental Physics I, University of Leipzig, Leipzig, Germany
E-mail: valiullin@uni-leipzig.de

New Journal of Physics **13** (2011) 015008 (19pp)
Received 3 August 2010
Published 28 January 2011
Online at http://www.njp.org/
doi:10.1088/1367-2630/13/1/015008

Abstract. Nuclear magnetic resonance (NMR) provides a variety of tools for the structural characterization of porous solids. In this paper, we discuss a relatively novel approach called NMR cryodiffusometry, which is based on a simultaneous assessment of both the phase state of intraporous liquids at low temperatures, using NMR cryoporometry, and their transport properties, using NMR diffusometry. Choosing two model porous materials with ordered and disordered pore structures as the host systems, we discuss the methodological and fundamental aspects of the method. Thus, with the use of an intentionally micro-structured mesoporous silicon, we demonstrate how its structural features give rise to specific patterns in the effective molecular diffusivities measured upon progressive melting of a frozen liquid in the mesopores. We then present the results of a detailed study of the transport properties of the same liquid during both melting and freezing processes in Vycor porous glass, a material with a random pore structure.

[1] Author to whom any correspondence should be addressed.

Contents

1. Introduction **2**
2. Materials and methods **3**
2.1. Porous materials 3
2.2. NMR measurements 4
3. Experimental results and discussion **6**
3.1. Ordered porous solids 6
3.2. Disordered porous solids 10
4. Conclusions **14**
Acknowledgments **15**
Appendix. Restricted diffusion between plates **15**
References **17**

1. Introduction

Porous solids have always been a focus of scientific research due to their extreme importance in diverse applications, such as catalysis, mass separation, pharmaceuticals and chromatography. To meet specific application-oriented purposes, a wide variety of porous materials have been synthesized, including microporous zeolites [1], mesoporous glasses [2] and macroporous silicon [3] as representative examples. In recent years, chemical synthesis has further progressed to provide various means to tailor the structural properties of porous solids [4]–[6] and to design complex, hierarchically organized porous matrices in a well-defined way. In this respect, one may refer to newly emerging classes of porous host materials, such as metal–organic frameworks [7] and porous coordination polymers [8]. In turn, such rapid growth of various types of porous materials consisting of several structural units with different internal porosities and pore morphologies, different spatial arrangements that may themselves give rise to quite different textural polymorphs, demands the appropriate development of experimental techniques for their structural characterization on different lengthscales.

Among a number of analytical methods serving this purpose, such as gas adsorption, mercury intrusion and x-ray diffraction, nuclear magnetic resonance (NMR) has long been recognized as a powerful tool non-invasively yielding information on various structural properties of porous host systems [9]–[11]. Thus, NMR relaxometry has been used to access specific surface area S/V and pore size distribution (PSD) [12], NMR cryoporometry to determine PSD [13] and pore shape [14], and NMR diffusometry to measure the S/V and tortuosity τ of porous solids [15] as well as pore shape [16]. One may further mention magnetic resonance imaging, revealing textural properties of materials on the macroscopic length scale [17].

One of the important properties of porous materials is the connectivity of the pore space. Some attempts at its quantification have earlier been made, based on analyses of gas sorption behavior [18, 19] and, in particular, desorption scanning behavior [20]. Alternatively, some information on interpore connectivity may be extracted from the tortuosity factor τ, a parameter accessible by pulsed field gradient (PFG) NMR. The tortuosity factor is defined as the ratio of the molecular diffusivity of a bulk fluid to the effective long-time diffusivity D_{eff} of the same fluid in a porous solid. Because D_{eff} is assessed by tracing the molecular displacements much

exceeding the typical pore size of the porous medium, τ does provide a value averaged over the whole structure. In this respect, new experimental approaches that can provide more local information, e.g. the degree to which different modes of a PSD function are connected to each other, are highly welcome.

Over the last few years, a few NMR-based approaches aimed at probing the local pore connectivities have been suggested. Among them, two-dimensional (2D) ^{129}Xe NMR exchange spectroscopy has successfully been employed to resolve different exchange pathways between pores of different sizes in electrochemically etched mesoporous silicon [21]. Similarly, but employing 2D NMR transverse relaxation exchange experiments, access to the pore–pore exchange properties of water in sandstone has been demonstrated [22]. In analogy to the work of Mason on gas desorption [20], NMR cryoporometry has also been shown to reveal similar details of pore space organization when the freezing pathways of liquids in mesopores are monitored [23].

Additionally, alternative approaches based on correlative studies of phase state and transport of fluids in mesopores have emerged [24]–[32]. In particular, NMR cryodiffusometry has been shown to potentially provide information on pore interconnectivity [24]–[26], [28, 30, 31]. The key idea of these types of experiments is continuous modification of the pore space of a porous solid via freezing or melting of the liquid in a certain subpopulation of the pores and tracing the diffusion behavior of the rest of the probe intrapore liquid. In the above-cited case studies, different aspects related to the overall phenomenon have been covered and the potential of this approach has been demonstrated. However, detailed experimental studies and respective theoretical descriptions are still lacking. In this paper, we present the results of our systematic experimental studies of two model porous systems providing an experimental basis for further theoretical analysis. By choosing materials with ordered and disordered pore structures, we offer instructive examples highlighting methodological aspects of the method, and discuss in more detail its applicability for material characterization.

2. Materials and methods

2.1. Porous materials

In this paper, two model porous materials with different morphologies of the pore space have been used to provide instructive examples and deeper insights into the method used. One of them, mesoporous silicon (PSi), has been chosen as a model material with ordered pore structure. It is typically prepared by electrochemical etching of silicon crystals [33]. By a proper choice of the etching conditions (etching current, temperature and electrolyte composition) and the initial material properties (dopant type and its concentration), PSi tablets (in our case with a diameter of a few cm and a thickness of a few tens of μm) with linear pores can be obtained [34]. In the present work, single-crystalline (100)-oriented p-type Si wafers with a resistivity of 2–5 mΩ cm were used. The electrolyte contained HF (48%) and C_2H_5OH in the ratio of 1 : 1. Micro-structuring was performed by a temporal modulation of the etching current density j during the fabrication between the three values of $j = 20\,\mathrm{mA\,cm^{-2}}$, $j = 60\,\mathrm{mA\,cm^{-2}}$ and $j = 120\,\mathrm{mA\,cm^{-2}}$ [35]. Note that etching steps with larger currents lead to larger pores. Two etching time schemes were used to produce the two structures shown in figure 1 (more information about the fabrication procedure may be found in [36]). For both materials, the overall PSi film thickness was about 48 μm. As a final step, to remove the PSi films from

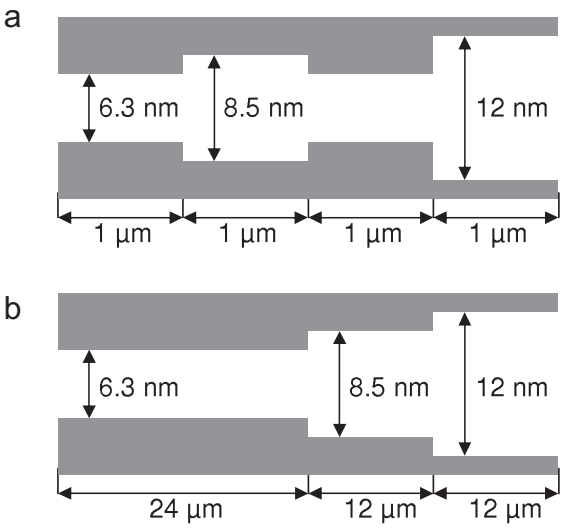

Figure 1. Schematic structure of the wo ordered mesoporous silicon samples used. The first material consisting of 12 repeating unit cells shown in (a) is referred to as the structured porous silicon. The unit cell is designed to have four sections of equal length of 1 μm and to have tubular pores with different average pore diameters. The pore diameters indicated in the figure were obtained using NMR cryoporometry as described in the text. The overall sample thickness of the thus prepared porous silicon film is 48 μm. Panel (b) shows a material referred to as the reference sample. It is designed to consist of the same pore volumes of the sections with a given pore structure as in the structured material in (a), but arranged to have only three large continuous sections with different structural properties.

the substrates, an electropolishing step with a current density of 700 mA cm^{-2} was applied for 2–3 s.

The second material studied was Vycor porous glass [37]. This is a classical representative of mesoporous materials with disordered pore structure. Structural characterization of Vycor porous glass is the subject of numerous previous studies [19, 20, 38, 39] and therefore this glass is often considered as a suitable, standard material for the comparison of experimental results obtained by different techniques and for validating theoretical models. For the purposes of this paper, it is sufficient to mention that it has a relatively low porosity of about 27% and a mean pore diameter of about 5–6 nm.

2.2. NMR measurements

^{1}H NMR studies were performed on a home-built spectrometer operating at 400 MHz for protons and equipped with a PFG unit [40]. All measurements, including measurements of both NMR signal intensities and molecular diffusivities, were carried out using the Hahn spin-echo pulse sequence [41]. The use of this pulse sequence for diffusion measurements under the conditions of our experiments is preferred due to the fact that the results obtained with the pulse sequences having, as a part, longitudinal magnetization-storage time periods, such as the stimulated or 13-interval sequences, can be distorted by nuclear cross-relaxation effects [42].

For NMR measurements, PSi chips have been stacked in a glass tube in such a way that the pore axes were aligned in the direction of the tube axis. This axis also coincided with the direction of the externally applied magnetic field gradient, ensuring, therefore, that the diffusion process of probe molecules along the main pore axis (recall their tubular morphology) is probed. Vycor porous glass was used in the form of a rod with a diameter of 6 mm and a length of 12 mm. The samples were initially outgassed and nitrobenzene, the probe liquid used in this study, was added at an amount to result in filling of all mesopores, with some excess amount covering the porous materials.

The protocol of the measurements was as follows. First, the temperature was slowly decreased to completely freeze nitrobenzene in the bulk state as well as in the pores. Notably, a strong supercooling, as compared to the bulk equilibrium transition temperature $T_0 \simeq 278.8\,\mathrm{K}$ for nitrobenzene, was observed. Thereafter, the temperature was increased in small steps, 15 minutes were given for the equilibration after each temperature increment and the spin-echo signal intensity was measured to compile the so-called melting curve. Upon reaching a temperature slightly below T_0, the direction of the temperature change was reverted to measure the freezing curve. In this way, one ensures that the frozen bulk nitrobenzene is present at the pore openings throughout all experiments and undesired supercooling effects leading to a delay of the homogeneous nucleation of the very first nuclei of the frozen phase in the mesopores can be avoided.

The freezing and melting processes were monitored via the spin-echo signal intensity measured with a typical interpulse delay $\tau = 3\,\mathrm{ms}$ between the radiofrequency pulses in the Hahn echo pulse sequence. This delay, which is chosen to be sufficiently longer than the transverse relaxation times in the frozen nitrobenzene phase (tens of microseconds), ensures almost complete suppression of the NMR signal from the frozen phase. It is worth noting that the data were corrected for both nuclear relaxation (dependence of the transverse relaxation rates T_2^{-1} on temperature) and Curie (dependence of the nuclear magnetization on temperature) effects [23].

To take into account the transverse relaxation weighting, we have used a strong supercooling observed on the cooling branch. This leads to a sufficiently broad temperature range where the intra-pore fluid is found in the supercooled liquid state. Thus, by measuring T_2-relaxation times of the supercooled nitrobenzene, one may use them to respectively normalize the spin-echo signal intensities measured during melting. Note, however, that such a correction is not strictly valid concerning liquid-like non-frozen layers, in which nuclear transverse relaxation times may have different behavior. Therefore, the low liquid fraction data have to be analyzed with care. The dependence of the nuclear magnetization on temperature was simply accounted for by multiplying the measured signal intensities by temperature. The corrected data, therefore, represent the signal intensity being proportional to the number of molecules in the liquid phase in the pores. The thus measured quantity may further be converted to a respective PSD, as described elsewhere [43, 44].

In addition to the NMR signal intensity, the diffusivities in the liquid phase were also measured after each temperature change. As mentioned, the measurements were carried out using the Hahn echo pulse sequence incorporating pulses of the magnetic field gradient with a typical duration δ of 500 μs and a strength g ranging from $g = 0\,\mathrm{T\,m^{-1}}$ to $g = 10\,\mathrm{T\,m^{-1}}$. In most cases, the thus measured spin-echo diffusion attenuation functions, i.e. the spin-echo intensity S versus the product $g^2\delta^2$, were of exponential shape. This dependence usually accompanies normal diffusion processes (diffusion propagator of Gaussian form) that, therefore, may be

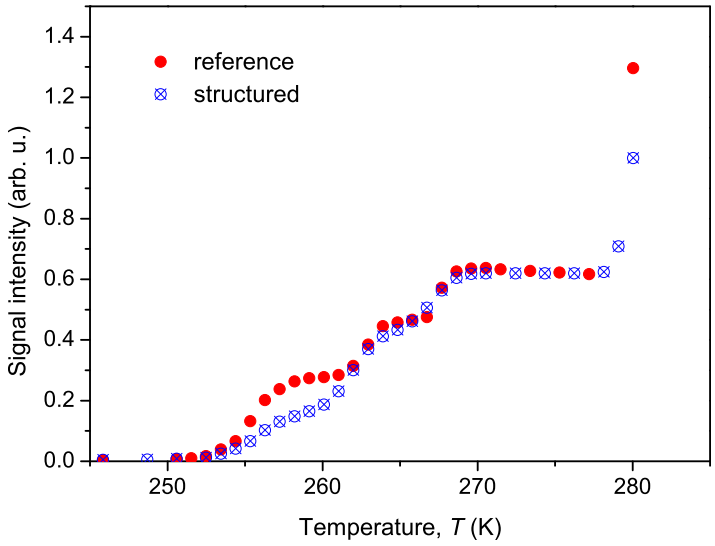

Figure 2. NMR signal intensities measured using the Hahn echo pulse sequence with $\tau = 3$ ms in the reference (filled circles) and structured (crossed circles) PSi samples as a function of temperature on the warming branch (melting curves).

described using a well-defined diffusivity. In this paper, we denote this diffusivity by D_{eff} and refer to it as an effective diffusivity. In the case of deviations of the spin-echo diffusion attenuations from the exponential shape, D_{eff} was obtained from the low $g^2\delta^2$ limit (for more details, see e.g. [29]).

3. Experimental results and discussion

3.1. Ordered porous solids

3.1.1. Phase transitions. We start our consideration with the seemingly most simple samples of PSi, containing pores of cylindrical morphology with intentionally varied pore diameters along the pore axis, as shown in figure 1. It has to be noted, however, that these drawings are, of course, idealized ones and it has recently been recognized that PSi materials obtained by electrochemical etching possess a substantial degree of pore-wall roughness. Consequently, it may have a considerable effect upon phase transitions. In fact, it was shown to result in, e.g., capillary condensation or evaporation transitions occurring in a way qualitatively similar to materials with disordered pore structure [45]–[47]. Despite the existence of such a disorder, the pores are still linear with a negligible number of interconnections between adjacent pores [46]. Also, the intentionally created structural patterns are not smeared out and are well observable [35]. In particular, they are clearly discernable in the melting curves shown in figure 2.

Upon warming the PSi samples, starting from the completely frozen state of nitrobenzene, a few steps in the melting curves are observed. The very last one, occurring at about 279 K, is associated with the melting of the bulk nitrobenzene surrounding the PSi chips (recall the presence of excess nitrobenzene). The three steps at about 255 , 263 and 268 K are formed due to the melting of nitrobenzene in the pore sections of PSi with different average pore diameters.

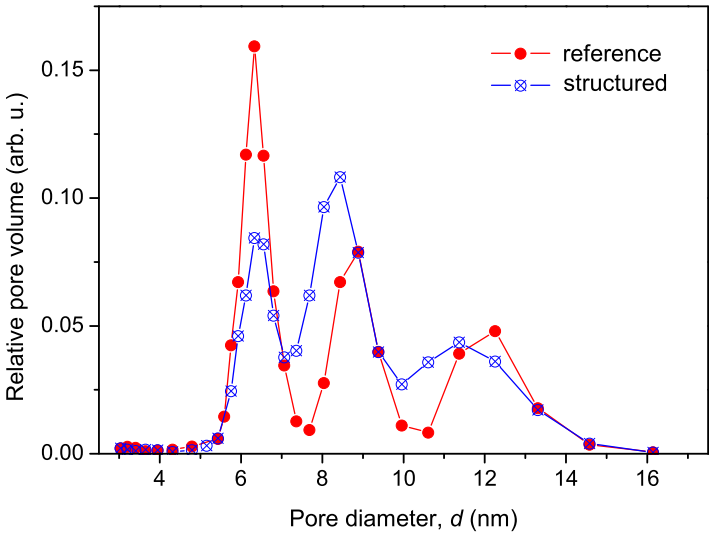

Figure 3. Pore size distributions of the reference (filled circles) and structured (open symbols) PSi samples obtained using NMR cryoporometry. To obtain these functions, the data of figure 2 were used. The lines shown are a guide to the eye.

According to the Gibbs–Thomson equation [48],

$$T_0 - T_m = K/d_c, \tag{1}$$

the melting temperature T_m of a crystal of a finite size d_c is inversely proportional to the crystal size and, therefore, to the pore diameter by which the dimension of the confined phase is limited. For liquids completely wetting the pore walls, the proportionality factor K is, in the first approximation, determined only by the physico-chemical properties of the confined liquid. Using this relationship, the data of figure 2 can readily be converted to the PSD functions that are presented in figure 3. The relevant details of this transformation can be found elsewhere [13, 43, 44]. Here we only note that we have used $T_0 = 278.8\,\mathrm{K}$ and $K = 125\,\mathrm{K\,nm}$ for nitrobenzene [35] and assumed that, between the frozen core and the pore walls of PSi, there exists one monolayer of nitrobenzene in a liquid-like state.

The thus obtained PSDs show three peaks, in full agreement with the structure expected from the fabrication procedure. Although both PSi samples, the reference and the structured ones, were designed to have identical relative volumes of different pore sections, some minor deviations are revealed by the measured PSDs. This can be caused either by some effects during etching (recall contact of the pore walls with the electrolyte during the fabrication and possible changes of the electrolyte concentration with etching time [36]) or by peculiarities of the melting transition due to a coupling between adjacent pore sections with pores of different dimensions.

3.1.2. Diffusion in the reference sample. The difference in the overall geometry of the samples, however, becomes clearly notable by measuring the effective diffusivities of the liquid phase along the melting curve. Figure 4 shows such data for both samples. For the reference sample, three regimes in the diffusive behavior may be identified. The temperature ranges corresponding to these regimes are well correlated with the features in the respective melting curves. Indeed,

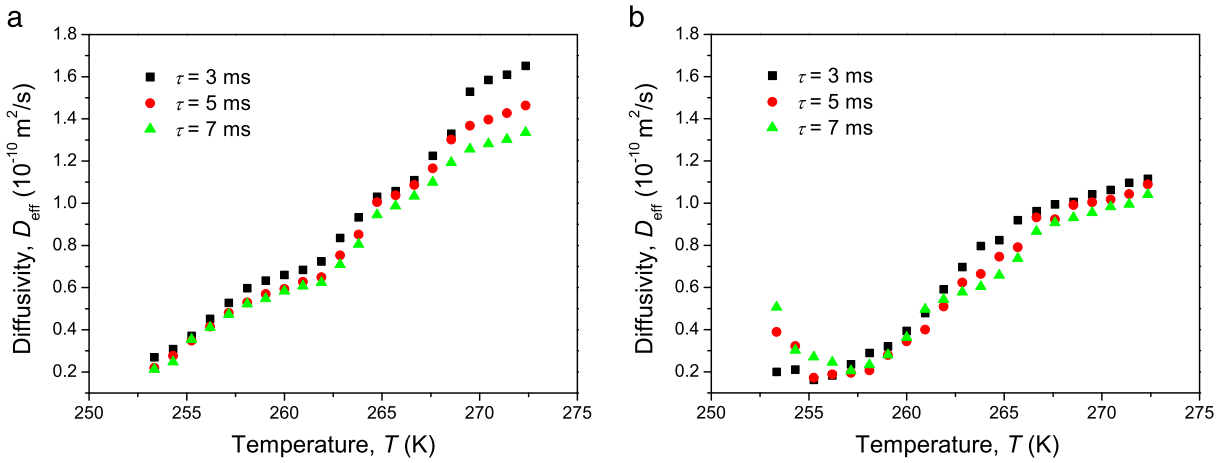

Figure 4. Effective diffusivities of nitrobenzene in (a) the reference and (b) the structured PSi samples measured simultaneously with the NMR signal intensities (figure 2) on the melting branch. The measurements have been carried out using three different interpulse separation times τ in the Hahn spin-echo pulse sequence, as indicated in the figures.

the stronger dependences of D_{eff} on temperature are found to correlate with the stronger increase in the signal intensity with temperature, i.e. where melting of the frozen phase does occur in the pore sections with a certain pore size. Similarly, the shoulders in figure 2 give rise to a weaker dependence of D_{eff} on T, presumably accounted for solely by an increase in the diffusivity in the liquid phase with increasing temperature (typically described by, e.g., the Arrhenius law).

The diffusivities of liquid nitrobenzene in PSi samples with tubular pores have previously been measured as a function of the average pore diameter [31]. It was found that the diffusivities increase with increasing pore diameter. One of the mechanisms leading to this behavior is the interaction of liquid molecules with the pore walls, tending to slow down the molecules at the surface. Thus, the overall diffusivity becomes a function of the surface-to-volume ratio, which increases with decreasing pore diameter. Based on the data of [31], it is expected that D_{eff} for the pores with average pore diameters of 6 and 12 nm differ by a factor of about 3. This finding satisfactorily explains a stronger increase in the diffusivities with increasing temperature in the regimes of the progressive melting as compared to the situation expected solely due to an increase in the kinetic energy with increasing temperature. Indeed, in agreement with the Gibbs–Thompson relation, pores with smaller pore size and, therefore, with smaller diffusivities of the intrapore liquids melt at lower temperatures.

In this material, the lengths (12 and 24 μm) of the sections containing pores with uniform pore diameters notably exceed the molecular displacements $\sqrt{D_{\mathrm{eff}}\tau}$ traced in our NMR experiments, which are found to be of the order of or below 1 μm. Hence, keeping in mind that all channels in PSi are parallel to each other [46] and diffusion is probed along the channel axes, the effects of restricted diffusion are not expected to play a role. This is further confirmed by the data from diffusion experiments performed with different interpulse delays τ in the Hahn echo pulse sequence, i.e. with different diffusion times, revealing only slight differences (except temperatures above 270 K). Thus, we experimentally prove that the transport properties of the molecular ensembles in the three different sections may be considered to be only slightly

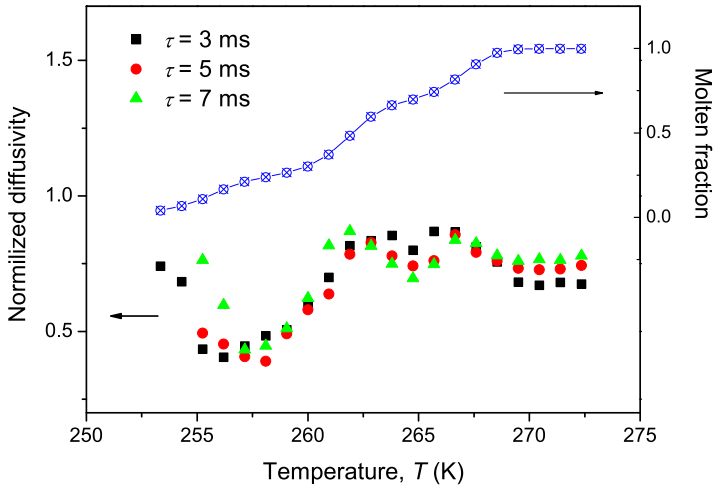

Figure 5. Normalized diffusivities for nitrobenzene in the structured PSi sample (left axis). For the normalization, the respective data obtained for the reference sample (the data of figure 4(a)) were used. The different symbols refer to the measurements performed with different times τ. Additionally, the data of figure 2 on melting of nitrobenzene in the structured porous silicon are shown by the crossed symbols (right axis). These data are normalized to the signal intensity measured when all mesopores contained liquid nitrobenzene but the excess liquid was frozen.

affected by the surrounding sections with differing structural characteristics. That is why we have referred to this sample as the reference.

3.1.3. Diffusion in the structured sample. Figure 4(b) shows the results of diffusion experiments performed with the structured PSi. It reveals additional features not observed for the reference material. In order to discern the solely structural properties of this sample, we normalize the data of figure 4(b) by those of figure 4(a). In this way, we may decouple the effects of pore space morphology on transport from those determined by an increase in the molecular kinetic energy (e.g. described by the Arrhenius law) and the dependence of D_{eff} on the pore size discussed in the preceding section. Notably, the latter two mechanisms contribute to the diffusion behavior in both PSi samples and, therefore, their effects may be canceled upon normalization. Thus the obtained data are shown in figure 5.

As a prominent feature of figure 5, the formation of minima and maxima may be noted. The position of the first minimum $T_{\mathrm{min},1}$, obtained at about 257 K, is nicely correlated with the temperature around which melting in the smallest pores, with an average diameter of 6.3 nm, is completed. We anticipate that the initial decrease in D_{eff} with increasing temperature up to $T_{\mathrm{min},1}$ is caused by the progressive formation of spatially continuous domains (or pore sections) containing liquid nitrobenzene. The pores in these sections, which are about 1 μm in length (see figure 1), are surrounded by larger pores containing frozen cores. Thus, in the domains containing molten nitrobenzene, diffusion will be restricted. As discussed in more detail in the appendix, an increase in temperature (and therefore in molecular mobilities) in this case will lead to a decrease in the normalized diffusivities.

In the adjacent pores, containing the frozen cores, the molecules may diffuse within the liquid-like layers of thickness $l_{n\mathrm{fl}}$ at the pore walls [49]. Thus, the domains containing molten nitrobenzene are connected to each other via such liquid-like layers. This may render the completely restricted diffusion model not valid. We anticipate, however, that for the $l_{n\mathrm{fl}}/d_p$ ratios sufficiently less than 1, which is presumably true in our experiments, the behavior will be qualitatively identical (also, see the discussion in the appendix). It is also worth noting that, as has been shown earlier, the adsorbing boundary conditions in this context have qualitatively similar effects to the effects of restricted diffusion [50]. Hence, if the molecules start their diffusion within the liquid domains and then, during the observation time, disappear from the NMR signal due to fast relaxation of the nuclear spins in the non-frozen liquid-like layers, this process will again result in a decrease in the measured diffusivities.

The increase in D_{eff} upon further warming up to a temperature of about 262 K, at which onset of melting is observed in pores of 8.5 nm diameter, may be associated with the increase of the thickness of the non-frozen surface layers with increasing temperature [51]. If the domains containing molten nitrobenzene stay intact, this process will lead to a respective increase in the permeability and, therefore, in the effective, long-range diffusivity. By approaching the porous medium as an arrangement of spherical cavities connected via cylindrical tubes with a smaller diameter, the phenomenon discussed may be considered as the result of an increase in the diameters of the connecting tubes, which is shown to lead to an increase in D_{eff} [52].

The occurrence of the second minimum at $T_{\mathrm{min},2} \approx 265$ K may be explained in a similar way, but now involving the formation of longer domains (with a length of 3 μm, according to figure 1) containing liquid nitrobenzene. This decrease, however, is less pronounced owing to the increase in both the size of the domains and the thickness of the non-frozen layers. Also, one may rationalize that the tortuosities of the two structures in figure 1 are different. As a consequence, this may account for the final slight decrease in D_{eff} during the melting of nitrobenzene in the biggest pores, as observed at temperatures above 267 K.

To summarize, using PSi as a model porous medium, we have shown that the effective diffusivities measured as a function of temperature during the melting of the intraporous frozen phase bear information on the structural features of the host material. Indeed, it is found that, upon proper normalization, well-resolved minima and maxima in the effective diffusivities are observed, which may further be nicely correlated with the structural features of the pore space. Because these features observed in the transport properties are closely interrelated with the differences in phase states of the fluid in the adjacent pores, further theoretical analysis using appropriate models is expected to yield unique information on the interconnectivity between these pores.

3.2. Disordered porous solids

By establishing how the structural features of ordered porous materials give rise to specific patterns in the diffusion behavior upon a continuous change in the pore space, it becomes interesting to see whether these patterns are still preserved in materials with random pore structures. To examine this, we have performed cryodiffusometry experiments with Vycor porous glass. It has to be noted that for intentionally structured samples, such as PSi, one can fabricate a 'reference' material related to it. As we have shown in the preceding section, this reference material, consisting of a collection of pores independent from each other with identical chemistries of the pore surface, may substantially help in singling out the structural

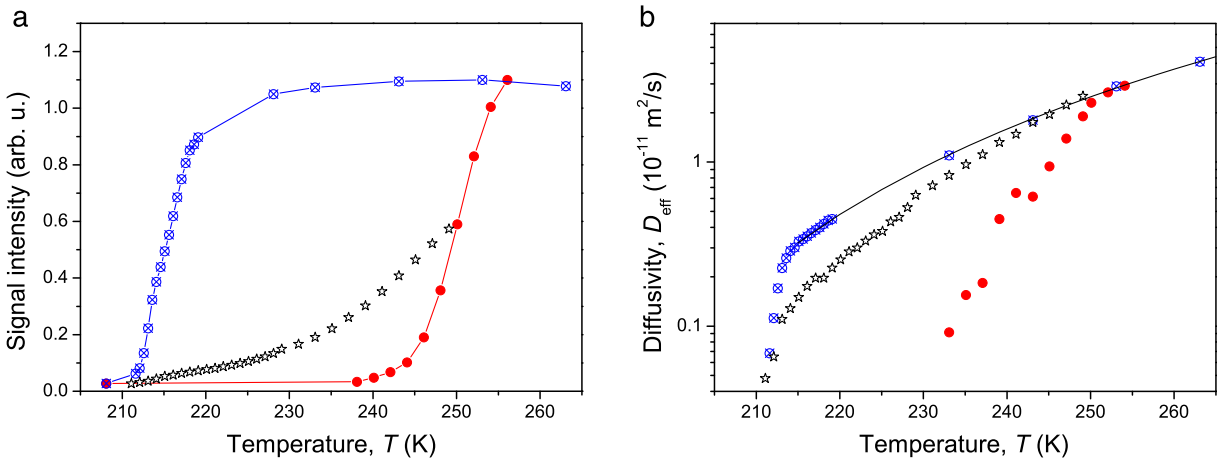

Figure 6. Freezing and melting curves (a) and the effective diffusivities (b) for nitrobenzene in Vycor porous glass as a function of temperature. The crossed and filled circles refer to the cooling (starting from the initial state at which all mesopores contain liquid nitrobenzene but excess nitrobenzene is frozen) and warming (starting from all nitrobenzene in the frozen state) branches, respectively. The open stars in panel (a) show the scanning freezing curve obtained by reverting the warming branch to the cooling one at a temperature at which still about 50% of the pore volume contains frozen nitrobenzene phase and in panel (b) the respective effective diffusivities obtained along with the scanning melting curve. In (a), the lines shown are a guide to the eye. In (b), the solid line shows a best fit of the Speedy–Angell equation (see text) to the diffusivity data measured on the cooling branch in the temperature range 218 –262 K.

properties of the material under study. To find such a reference material for porous solids, such as random glasses, including Vycor porous glass, is hardly possible. Therefore, we have used an alternative approach based on the consideration of the fluid properties in the pores during both cooling and warming branches.

Figure 6 shows the freezing and melting curves and the effective diffusivities of nitrobenzene in Vycor porous glass measured upon cooling and warming the system. First, we would like to point out the occurrence of a relatively broad freezing/melting hysteresis in figure 6(a). All possible mechanisms contributing to its formation have already been discussed in detail in our previous work [23]. In particular, the delayed metastable freezing has been associated with a strong pore-blocking effect. The latter becomes evident, e.g., by comparing the data on freezing obtained by cooling from the completely molten state and the state with only half of the mesopores containing liquid phase (see figure 6(a)). Irrespective of specific details, NMR cryodiffusometry experiments may profit from the occurrence of strong supercooling in the mesopores. Indeed, the data on the diffusivities of the supercooled liquid recorded on the cooling branch, resulting without any confinement by a frozen phase, may be used for the normalization of the effective diffusivities measured during melting. In this way, the variation in D_{eff} with temperature due to the change in the molecular kinetic energy may be removed.

In line with the freezing/melting hysteresis, a hysteresis between the effective diffusivities measured on cooling and warming is observed as expected. To further analyze these data, we

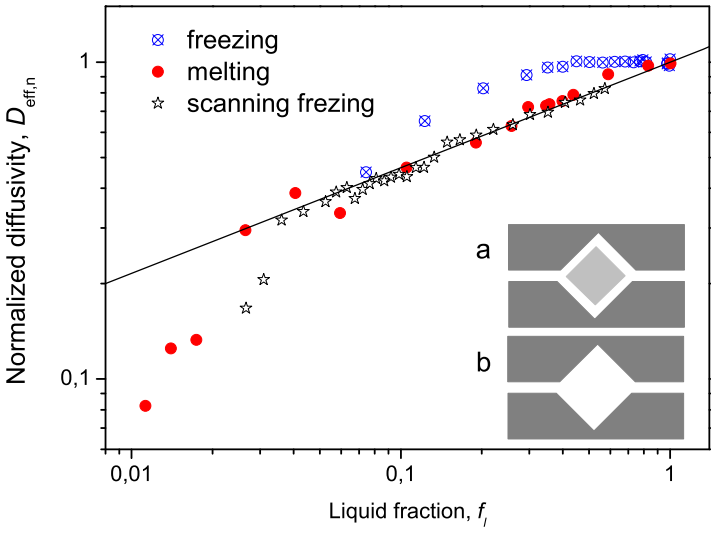

Figure 7. Normalized diffusivities $D_{\mathrm{eff},n}$ for nitrobenzene in Vycor porous glass as a function of the liquid fraction f_l of nitrobenzene in the mesopores during freezing (crossed circles) and melting (filled circles) from the completely molten and frozen states, respectively, and during scanning freezing (open stars) from the half-molten state (see figure 6 for a more detailed explanation). For the normalization, the diffusivities of figure 6(b) were divided by the respective diffusivities in the supercooled state (solid line in figure 6(b)). The solid line shows the power-law function $f_l^{1/3}$. The inset shows a model structure explaining the observation of the minimum in $D_{\mathrm{eff},n}$ at $f_l \approx 0.06$. In (a), only the non-frozen surface layers (shown in white) are accessible for diffusion. In (b), the formation of the domain containing liquid leads to increasing tortuosity and, therefore, to decreasing effective diffusivity.

will normalize the diffusivities in a way discussed in the preceding paragraph and plot them versus the relative fraction f_l of the liquid phase. First, we fit the data on D_{eff} measured on the cooling branch in the temperature range from 260 to 220 K to some analytical equation and then use it for the normalization. We found that the Speedy–Angell equation [53],

$$D_{sl}(T) = D_{s0}\left(\frac{T}{T_s} - 1\right)^k, \tag{2}$$

suits our purposes reasonably well. The best fit to the experimental data is found with $D_{s0} = 4.1 \times 10^{-10}\,\mathrm{m^2\,s^{-1}}$, $T_s = 181.8\,\mathrm{K}$ and $k = 2.85$. The normalized diffusivities $D_{\mathrm{eff},n}$ are then defined as $D_{\mathrm{eff},n} = D_{\mathrm{eff}}/D_{sl}$. In figure 7, $D_{\mathrm{eff},n}$ are plotted as a function of f_l, where for the temperature–liquid fraction transformation the data of figure 6(a) were used.

The thus plotted data on $D_{\mathrm{eff},n}$ clearly reveal a few interesting features. First of all, a notable hysteresis is still preserved between the data on freezing and melting. This phenomenon has already been reported earlier for two-phase systems in porous solids, including both liquid–gas [54, 55] and solid–liquid equilibrium [31]. A clue to understand it in our particular case is provided by the data obtained upon cooling, showing almost no dependence of $D_{\mathrm{eff},n}$ on the liquid fraction f_l down to about $f_l = 0.3$. This finding is most straightforwardly explained by

the invasion-percolation character of the freezing process in Vycor porous glass, as established in our previous work [23]. Indeed, in such small pores of less than 10 nm, the process of homogeneous nucleation is strongly suppressed. On the other hand, at the pore openings, there is a direct contact of the intrapore liquid with the frozen bulk nitrobenzene. This facilitates freezing via the solid front penetration from the particle boundaries into the porous solid. Recalling the macroscopic dimension of the Vycor porous glass particle used (a few mm), it becomes clear that the liquid phase in the particle core forms a continuous domain with a size notably exceeding the molecular displacements of up to 1 μm, as registered in the experiments. Therefore, the diffusion process on the length scales as probed by PFG NMR appears to be unaffected, i.e. not restricted by the frozen domains down to $f_l = 0.3$.

In contrast to freezing, it is believed that melting occurs homogeneously over the entire volume of the particle. Before the very first liquid domains could be formed, the measured diffusivities may be associated with the mobility of nitrobenzene in the non-frozen surface layers [49]. In figure 7, these are the data points for f_l less than about 0.05. This conclusion we draw solely based on the fact that for $f_l < 0.05$, $D_{\mathrm{eff},n}(f_l)$ behaves differently from the case of higher liquid fractions. It has to be noted, however, that the normalization has been done taking into account the temperature dependence of diffusion behavior in the supercooled liquid. The respective behavior in the non-frozen layers may be different and, therefore, the data for the region $f_l < 0.05$ may have only qualitative meaning. In addition, in this region it is not trivial to properly take into account nuclear relaxation effects, which shift the values of f_l from the real ones.

Upon further warming, spatially separated domains of the liquid phase appear homogeneously distributed in the pore space, in agreement with the Gibbs–Thompson criterion given by equation (1). Their typical dimension may be estimated to be about a few tens of nm [38]. The occurrence of such domains is evidenced by the observation of a minimum in $D_{\mathrm{eff},n}$ at $f_l \approx 0.06$–0.08. Here, we would like to mention that this is not just a scatter in the data shown in the figure, but this phenomenon was systematically observed by repeating these experiments. Because of nuclear relaxation effects, resulting in the apparent values of f_l that may deviate from the real ones, their direct comparison to f_l obtained from calculations of relative volumes occupied by the liquid phase based on the geometrical characteristics of the pore space may not be correct in this region.

The mechanism of the minimum formation is presumably identical to that discussed in relation to figure 5, i.e. the restriction of diffusion in the liquid-filled domains, poorly connected to each other via the non-frozen layers in the pores containing the frozen core. Alternatively, this may be explained by noting that upon forming such molten domains, the tortuosity increases, decreasing, in turn, the effective diffusivity. This may easily be rationalized by considering a simple model, as shown in the inset of figure 7. Obviously, the tortuosity of the liquid phase in model (a), modeling the existence of only non-frozen surface layers, is higher as compared to that of the model (b), where the region of the frozen core is now accessible for diffusion.

Further growth of these domains with increasing temperature is, presumably, determined by the probability of their statistical clustering. Keeping in mind our limited understanding of the thermodynamics of mesoscalic systems, we cannot exclude growth of the initially formed domains of the liquids phase by moving the solid–liquid interface in the direction of the pore axis. Nevertheless, the domains of liquid phase formed during melting have mesoscalic dimensions throughout the experiments, resulting in slower diffusivities as compared to those obtained on the freezing branch at identical f_l.

It is very informative to compare the data on the effective diffusivities obtained along the melting curve (filled circles in figure 7) and the scanning freezing curve (open stars in figure 7), which are found to coincide within experimental error. This finding reveals that, upon removing kinetic limitations for the nucleation processes, the phase composition in random materials plays a decisive role in determining D_{eff}. However, a particular functional dependency of the diffusivities on f_{l} still contains information on the pore space organization. Although the fine details of the geometrical configuration of the phases remain screened in these types of experiments, we anticipate that they can be assessed by performing 2D NMR transverse relaxation exchange spectroscopy studies [22] during partial melting and freezing scans.

A better understanding of the overall behavior of $D_{\mathrm{eff},n}(f_l)$ in the range of liquid fractions $0.1 < f_{\mathrm{l}} < 1$ may be achieved upon considering theoretical models taking into account a particular spatial distribution (random, in the first instance, or chosen according to some two-point correlation function [56]) of pores with different pore sizes and their interconnectivity. An alternative strategy might be an analysis based on the well-known Archie law, which was often employed for the analysis of similar systems [57, 58]. The use of the Archie law may be justified by noting that the data in figure 7 in the region of interest are well reproduced by a power law. Taking into account, however, the limited range of normalized diffusivities over which they vary, a reliable proof of the validity of this assumption is far from trivial.

4. Conclusions

Accessing the structural details of porous solids is an important task of material-characterization sciences. Among a number of experimental techniques, NMR cryodiffusometry has recently emerged as a powerful method yielding unique information on the pore-space organization, including pore-space interconnectivity. It is essentially based on a simultaneous probing of the processes of molecular diffusion and of freezing and/or melting using NMR.

In the present paper, by profiting from our ability to produce mesoporous material with well-defined structured properties, we demonstrate and discuss in detail the correlation between the details of molecular spatial propagation and the structural features of the pore space where the diffusion does occur. Importantly, the porous space is continuously modified by adding/removing rigid domains of the frozen phase accomplished on the basis of the size dependence of first-order phase transitions. By the use of the most simple model pore structures, we make it easily recognizable how the phenomenon of restricted diffusion gives rise to such correlations. With all structural information known in advance, these results provide a stimulating and elaborated compilation of experimental data which may be compared directly to theoretical models.

As a step further, we present the results of a systematic study of transport and solid–liquid phase equilibrium in Vycor mesoporous glass with random pore structure. The data obtained for this material reveal a pronounced hysteresis between the diffusivities of the probe liquid measured on cooling and warming branches and compared at the identical phase compositions of the frozen and liquid phases in the mesopores. This finding contributes further to a fundamental understanding of phase transition processes under confinement in random mesopores and confirms the existence of different pathways of crystal growth and shrinking during freezing and melting, respectively. The molecular diffusivities analyzed as a function of the phase composition reveal two distinct regimes associated with the molecular propagation within the non-frozen surface layers and an admixture of the diffusion processes in those layers

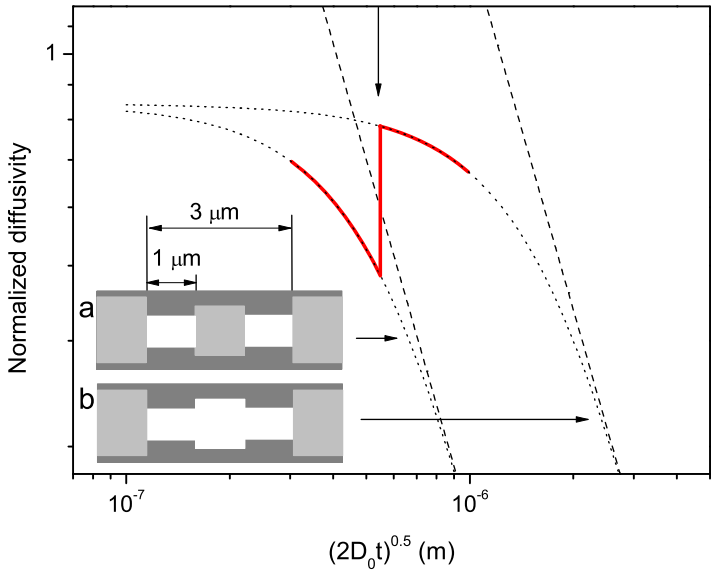

Figure A.1. Normalized diffusivities D_{cr}/D_0 (dotted lines) of a liquid in an idealized model of the structured porous silicon as a function of molecular displacements $r = (2D_0(T)t)^{1/2}$ calculated via equation (A.1). The dashed lines show the long-time asymptotes given by $D_{cr}/D_0 = L^2/6r$. The variation in the normalized diffusivities one would measure upon changing the temperature and therefore r (due to temperature-dependent D_0) and keeping $t = 3$ ms fixed is visualized by the solid line (refer to the main text for more details). The vertical arrow shows r corresponding to temperature T_2. The inset depicts a model of the structured porous silicon containing frozen liquid (shown in light gray) and molten liquid (shown in white). The configurations (a) and (b) are attained at temperatures T_1 and T_2 upon warming, respectively.

and in the progressively building up domains of the liquid phase. The results of a theoretical modeling of these processes will be the subject of our forthcoming publication.

Acknowledgments

This work was supported by the German Research Foundation (DFG), in particular in the framework of the Saxonian Research Group, FOR 877 'From local constraints to macroscopic transport'.

Appendix. Restricted diffusion between plates

Let us consider an idealized pore structure, as shown in the inset of figure A.1, modeling the geometry of the structured porous silicon sample used in the present study. Let us assume that at low temperatures the liquid freezes completely, i.e. non-frozen, liquid-like layers adjacent to the pore walls are not formed and also they do not form upon warming. With increasing temperature, first the frozen liquid melts in the sections with smallest diameter d_1 at a temperature $T_1 = K/d_1$.

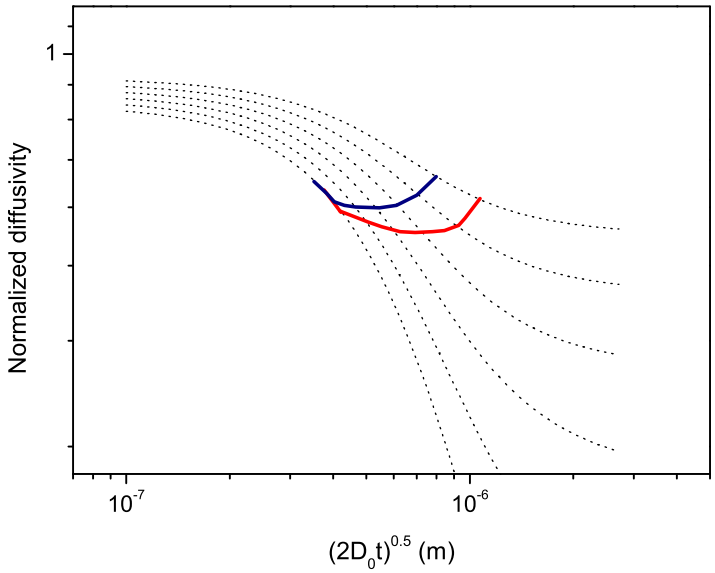

Figure A.2. Normalized diffusivities $D_n = D_{cr}/D_0$ (dotted lines) of a liquid in an idealized model of the structured porous silicon containing frozen domains, as depicted in the inset (a) of figure A.1, as a function of molecular displacements. The difference with the data on D_n of figure A.1 results from taking into account the existence of non-frozen, liquid-like layers between the frozen core and the pore walls: the higher the curve, the higher their thickness. The solid lines show possible pathways of D_n with increasing temperature.

The corresponding situation is shown in the inset (a). Note that because we do not allow for non-frozen, liquid-like layers, diffusion in the thus formed liquid domains will become completely restricted at sufficiently long times. The respective time-dependent diffusion coefficient $D_{cr}(t)$ along the pore axis can in this case be readily found analytically [59],

$$D_{cr}(t) = \frac{L^2}{2t}\left[\frac{1}{6} - 16\sum_{m=0}^{\infty}\frac{1}{(2m+1)^4\pi^4}\exp\left\{-(2m+1)^2\pi^2\frac{D_0 t}{L^2}\right\}\right], \tag{A.1}$$

where L is the length of the section where diffusion does occur and D_0 is the diffusivity along the pore axis in an infinitely long channel. With further increase in temperature, the middle sections (as shown in the inset (b) of figure A.1) will melt at a temperature T_2. Importantly, the diffusion process in the thus formed liquid domains will be described by equation (A.1), but with increased L. Thus, it appears that L in this particular problem might be considered as a temperature-dependent, stepwise function. It has to be mentioned that we neglect a minor change in D_0 due to the modulation of the pore diameter along the pore axis.

Figure A.1 shows the normalized diffusivity $D_n = D_{cr}/D_0$, as calculated using equation (A.1) for two values of $L = 1\,\mu$m and $L = 3\,\mu$m, as a function of molecular displacements. The latter is defined as $r = (2D_0(t))^{1/2}$ and is a function of both the diffusion time t and the diffusivity D_0. The diffusion time t, which is given in our experiments by τ, is held constant. D_0, however, changes with changing temperature and, therefore, gives rise to the respective variation of r. Thus, according to figure 4(a), in the temperature interval studied from

about 252 to 272 K, D_0 varies from about 2×10^{-11} to 1.4×10^{-10} m^2 s^{-1}. Using $\tau = 3$ ms, this corresponds to molecular displacements r from about 0.3 to 0.9 μm.

Finally, to find the normalized diffusivities in this range of r, we can use equation (A.1), explicitly taking into account the temperature-dependent behavior L. The result is shown in figure A.1 by the solid line, which is reminiscent of the experimentally observed behavior in figure 5. It is worth pointing out two opposite trends giving rise to this behavior: (i) the decrease in D_n with increasing temperature is due to increasing molecular displacements, resulting in a stronger effect of restrictions as given by equation (A.1), and (ii) the growth of liquid-containing domains with increasing temperature leads, in contrast, to an increase in D_n. Altogether, the analysis performed with this idealized model reveals that the combined effects of restricted diffusion in regions with temperature-dependent dimensions and of temperature-dependent variation of the molecular displacements may give rise to the formation of minima and maxima in the normalized diffusivities probed with increasing temperature.

Modeling the impact of non-frozen, liquid-like layers on the effective diffusivities is not trivial. Generally, their existence leads to the occurrence of finite diffusivities D_∞ at molecular diffusivities much exceeding typical sizes of the domains of the liquid phase. The thickness $l_{n\mathrm{fl}}$ of these layers evidently depends on temperature [51]. Thus, it is reasonable to expect that D_∞ will increase with increasing $l_{n\mathrm{fl}}$ in other identical conditions. Such behavior is shown schematically in figure A.2. It now becomes clear that with increasing temperature an interplay of two mechanisms, namely of restricted diffusion, tending to decrease D_n, and of increasing $l_{n\mathrm{fl}}$, tending to increase D_n, will determine a particular pathway of D_n. As an example, the solid lines in figure A.2 show two such pathways.

References

[1] Weitkamp J, Karge H G, Pfeifer H and Hörderlich W 1994 *Zeolites and Related Microporous Materials: State of the Art* (Amsterdam: Elsevier)

[2] Enke D, Janowski F and Schwieger W 2003 Porous glasses in the 21st century—a short review *Microporous Mesoporous Mater.* **60** 19–30

[3] Matthias S, Müller F, Schilling J and Gösele U 2005 Pushing the limits of macroporous silicon etching *Appl. Phys.* A **80** 1391–6

[4] Barton T J *et al* 1999 Tailored porous materials *Chem. Mater.* **11** 2633–56

[5] Coppens M-O, Sun J and Maschmeyer T 2001 Synthesis of hierarchical porous silicas with a controlled pore size distribution at various length scales *Catal. Today* **69** 331–5

[6] Schüth F and Schmidt W 2002 Microporous and mesoporous materials *Adv. Mater.* **14** 629–38

[7] Yaghi O M, O'Keeffe M, Ockwig N W, Chae H K, Eddaoudi M and Kim J 2003 Reticular synthesis and the design of new materials *Nature* **423** 705–14

[8] Kitagawa S, Kitaura R and Noro S 2004 Functional porous coordination polymers *Angew. Chem., Int. Ed. Engl.* **43** 2334–75

[9] Watson A T and Chang C T P 1997 Characterizing porous media with NMR methods *Prog. Nucl. Magn. Reson. Spectrosc.* **31** 343–86

[10] Stallmach F and Kärger J 1999 The potentials of pulsed field gradient NMR for investigation of porous media *Adsorpt.—J. Int. Adsorpt. Soc.* **5** 117–33

[11] Song Y-Q, Cho H, Hopper T, Pomerantz A E and Sun P Z 2008 Magnetic resonance in porous media: recent progress *J. Chem. Phys.* **128** 052212–2

[12] Bhattacharja S, Dorazio F, Tarczon J C, Halperin W P and Gerhardt R 1989 Internal structure of porous silica—a model system for characterization by nuclear magnetic resonance *J. Am. Ceram. Soc.* **72** 2126–30

[13] Strange J H, Rahman M and Smith E G 1993 Characterization of porous solids by NMR *Phys. Rev. Lett.* **71** 3589–91
[14] Petrov O and Furó I 2006 Curvature-dependent metastability of the solid phase and the freezing-melting hysteresis in pores *Phys. Rev.* E **73** 011608
[15] Mitra P P, Sen P N, Schwartz L M and Ledoussal P 1992 Diffusion propagator as a probe of the structure of porous media *Phys. Rev. Lett.* **68** 3555–8
[16] Shemesh N, Ozarslan E, Adiri T, Basser P J and Cohen Y 2010 Noninvasive bipolar double-pulsed-field-gradient NMR reveals signatures for pore size and shape in polydisperse, randomly oriented, inhomogeneous porous media *J. Chem. Phys.* **133** 044705
[17] Stapf S and Han S 2005 *NMR Imaging in Chemical Engineering* (Weinheim: Wiley-VCH)
[18] Mason G 1982 The effect of pore-space connectivity on the hysteresis of capillary condensation in adsorption desorption isotherms *J. Colloid Interface Sci.* **88** 36–46
[19] Page J H, Liu J, Abeles B, Deckman H W and Weitz D A 1993 Pore–space correlations in capillary condensation in Vycor *Phys. Rev. Lett.* **71** 1216–9
[20] Mason G 1988 Determination of the pore-size distributions and pore–space interconnectivity of vycor porous-glass from adsorption desorption hysteresis capillary condensation isotherms *Proc. R. Soc.* A **415** 453–86
[21] Knagge K, Smith J R, Smith L J, Buriak J and Raftery D 2006 Analysis of porosity in porous silicon using hyperpolarized XE-129 two-dimensional exchange experiments *Solid State Nucl. Magn. Reson.* **29** 85–9
[22] Washburn K E and Callaghan P T 2006 Tracking pore to pore exchange using relaxation exchange spectroscopy *Phys. Rev. Lett.* **97** 175502–4
[23] Kondrashova D, Reichenbach C and Valiullin R 2010 Probing pore connectivity in random porous materials by scanning freezing and melting experiments *Langmuir* **26** 6380–5
[24] Filippov A V, Altykis M G, Khaliullin M I, Rachimov R Z and Lantsov V M 1996 Study of the porous structure of hardened gypsum by pulsed nuclear magnetic resonance *J. Mater. Sci.* **31** 4369–74
[25] Filippov A V and Skirda V D 2000 An investigation of the structure of a porous substance by NMR cryodiffusometry *Colloid J.* **62** 759–64
[26] Valiullin R and Furó I 2002 Low-temperature phase separation of a binary liquid mixture in porous materials studied by cryoporometry and pulsed-field-gradient NMR *Phys. Rev.* E **66** 031508
[27] Valiullin R, Kortunov P, Kärger J and Timoshenko V 2004 Concentration-dependent self-diffusion of liquids in nanopores: a nuclear magnetic resonance study *J. Chem. Phys.* **120** 11804–14
[28] Perkins E L, Rigby S P, Edler K J and Lowe J 2007 Nmr cryoporometry and pfg studies of water diffusion in poly(lactic-co-glycolic acid) microspheres for drug delivery *J. Pharm. Pharmacol.* **59** A17
[29] Valiullin R, Dvoyashkin M, Kortunov P, Krause C and Kärger J 2007 Diffusion of guest molecules in MCM-41 agglomerates *J. Chem. Phys.* **126** 054705–6
[30] Perkins E L, Lowe J P, Edler K J, Tanko N and Rigby S P 2008 Determination of the percolation properties and pore connectivity for mesoporous solids using NMR cryodiffusometry *Chem. Eng. Sci.* **63** 1929–40
[31] Dvoyashkin M, Khokhlov A, Valiullin R and Kärger J 2008 Freezing of fluids in disordered mesopores *J. Chem. Phys.* **129** 154702–6
[32] Valiullin R, Kärger J and Gläser R 2009 Correlating phase behaviour and diffusion in mesopores: perspectives revealed by pulsed field gradient NMR *Phys. Chem. Chem. Phys.* **11** 2833–53
[33] Canham L T 1990 Silicon quantum wire array fabrication by electrochemical and chemical dissolution of wafers *Appl. Phys. Lett.* **57** 1046–8
[34] Parkhutik V 1999 Porous silicon—mechanisms of growth and applications. *Solid State Electron.* **43** 1121–41
[35] Khokhlov A, Valiullin R, Kärger J, Steinbach F and Feldhoff A 2007 Freezing and melting transitions of liquids in mesopores with ink-bottle geometry *New J. Phys.* **9** 272
[36] Khokhlov A 2009 Nanoporous silicon: structural characterization using NMR and applications *PhD Thesis* University of Leipzig
[37] Elmer T H 1992 Porous and reconstructed glasses *Engineered Materials Handbook* vol 4 (Materials Park, OH: ASM International) p 427–32

[38] Wiltzius P, Bates F S, Dierker S B and Wignall G D 1987 Structure of porous Vycor glass *Phys. Rev.* A **36** 2991–4
[39] Levitz P, Ehret G, Sinha S K and Drake J M 1991 Porous vycor glass: the microstructure as probed by electron microscopy, direct energy transfer, small-angle scattering, and molecular adsorption *J. Chem. Phys.* **95** 6151–61
[40] Galvosas P, Stallmach F, Seiffert G, Karger J, Kaess U and Majer G 2001 Generation and application of ultra-high-intensity magnetic field gradient pulses for NMR spectroscopy *J. Magn. Reson.* **151** 260–8
[41] Stejskal E O and Tanner J E 1965 Spin diffusion measurements—spin echoes in presence of a time-dependent field gradient *J. Chem. Phys.* **42** 288–92
[42] Valiullin R and Furó I 2002 The morphology of coexisting liquid and frozen phases in porous materials as revealed by exchange of nuclear spin magnetization followed by H-1 nuclear magnetic resonance *J. Chem. Phys.* **117** 2307–16
[43] Mitchell J, Beau J, Webber W and Strange J H 2008 Nuclear magnetic resonance cryoporometry *Phys. Rep.* **461** 1–36
[44] Petrov O V and Furó I 2009 NMR cryoporometry: principles, applications and potential *Prog. Nucl. Magn. Reson. Spectrosc.* **54** 97–122
[45] Wallacher D, Kunzner N, Kovalev D, Knorr N and Knorr K 2004 Capillary condensation in linear mesopores of different shape *Phys. Rev. Lett.* **92** 195704
[46] Naumov S, Khokhlov A, Valiullin R, Kärger J and Monson P A 2008 Understanding capillary condensation and hysteresis in porous silicon: network effects within independent pores *Phys. Rev.* E **78** 060601–4
[47] Naumov S, Valiullin R, Kärger J and Monson P A 2009 Understanding adsorption and desorption processes in mesoporous materials with independent disordered channels *Phys. Rev.* E **80** 031607
[48] Jackson C L and McKenna G B 1990 The melting behavior of organic materials confined in porous solids *J. Chem. Phys.* **93** 9002–11
[49] Stapf S and Kimmich R 1997 Translational mobility in surface induced liquid layers investigated by NMR diffusometry *Chem. Phys. Lett.* **275** 261–8
[50] Frey S, Kärger J, Pfeifer H and Walther P 1988 NMR self-diffusion measurements in regions confined by absorbing walls *J. Magn. Reson.* **79** 336–42
[51] Petrov O V, Vargas-Florencia D and Furó I 2007 Surface melting of octamethylcyclotetrasiloxane confined in controlled pore glasses: curvature effects observed by 1H NMR *J. Phys. Chem.* B **111** 1574–81
[52] Berezhkovskii A M, Zitserman V Y and Shvartsman S Y 2003 Diffusivity in periodic arrays of spherical cavities *J. Chem. Phys.* **118** 7146–7
[53] Speedy R J and Angell C A 1976 Isothermal compressibility of supercooled water and evidence for a thermodynamic singularity at −45 °C *J. Chem. Phys.* **65** 851–8
[54] Valiullin R, Naumov S, Galvosas P, Kärger J, Woo H J, Porcheron F and Monson P A 2006 Exploration of molecular dynamics during transient sorption of fluids in mesoporous materials *Nature* **443** 965–8
[55] Naumov S, Valiullin R, Galvosas P, Kärger J and Monson P A 2007 Diffusion hysteresis in mesoporous materials *Eur. Phys. J. Spec. Top.* **141** 107–12
[56] Jiao Y, Stillinger F H and Torquato S 2007 Modeling heterogeneous materials via two-point correlation functions: basic principles *Phys. Rev.* E **76** 031110–5
[57] Ardelean I, Mattea C, Farrher G, Wonorahardjo S and Kimmich R 2003 Nuclear magnetic resonance study of the vapor phase contribution to diffusion in nanoporous glasses partially filled with water and cyclohexane *J. Chem. Phys.* **119** 10358–62
[58] Han M, Youssef S, Rosenberg E, Fleury M and Levitz P 2009 Deviation from Archie's law in partially saturated porous media: wetting film versus disconnectedness of the conducting phase *Phys. Rev.* E **79**
[59] Sen P N 2004 Time-dependent diffusion coefficient as a probe of geometry *Concepts Magn. Reson.* A **23** 1–21